Detection of the Galactic 21 cm Line Using CHART Horn Antenna

November 2025

1. Introduction and Background

The 21 cm hyperfine transition of neutral hydrogen (HI) is the primary tracer of large-scale Galactic structure Basu et al. (2022). Its rest frequency is 1420.40575 MHz and, for the Milky Way, the intrinsic line widths are set by thermal broadening, turbulence, and Galactic rotation. A student-built instrument such as the CHART horn antenna consisting of a conical waveguide, a tuned feed, low-noise amplification, and an SDR backend is sufficient to detect the bright Galactic HI signal when properly tuned, impedance matched, and calibrated.

The goal of this experiment was to "point-and-shoot" which means direct the horn toward selected sky positions along or near the Galactic plane, acquire raw spectra with an RTL-SDR or FieldFox device, and recover the 21 cm line through standard post-processing (bandpass correction, averaging, and RFI inspection). We follow (Berkhout et al. 2023), which describes the CHART build, feed tuning, RFI environment, and the detection pipeline. We also make use of code in CHART GitHub repository [1] for the postprocessing of the raw data.

Our task: (1) set up the horn on five different days using two feed designs (cardboard prototype and metal horn), (2) examine how RFI sources, feed mismatch, and site geometry affect the detected spectrum, (3) measure and interpret the appearance or absence of a spectral line near 1420 MHz, (4) record coordinates of successful pointings, and (5) generate a HI emission map.

2. Experimental Setup

Antenna and Feed. Two horn variants were used - a cardboard prototype and a metal horn. The feed consisted of a wire probe inside a coaxial connector. Prior to Day 4, the feed was mistuned: the probe length corresponded roughly to ~ 900 MHz resonance rather than 1420 MHz. Measured return loss indicated $\sim 70\%$ of the incident power being reflected. Retuning the probe to half the previous length reduced reflection to $\sim 1\%$.

Electronics. Observations used two configurations:

- Figure 1: Low-Noise Amplifier (LNA)+Raspberry Pi + RTL-SDR (Day 1,3,4), with 10 s integration time and 5 iterations per frequency bin.
- Keysight FieldFox spectrum analyzer (Day 2).

Data Processing. Each raw dump consisted of multiple SDR "trials" per pointing. For every trial, the time–frequency data array was averaged along the time axis to obtain a single 1D power spectrum. The spectrum was then converted to decibels and trimmed by removing approximately 1/16 of the channels at both ends to exclude regions affected by filter roll-off. Frequency axes were reconstructed from the SDR metadata using the sample rate, center frequency, and vector length, and converted to GHz. A per-pointing bandpass correction was applied by dividing each spectrum by the pre-computed bandpass function *bps*[pointing] prior to the $\log_{10}$ transform. Because the SDR collects data in adjacent frequency chunks with small overlaps, successive spectra were stitched together by aligning their overlapping frequency

[1] https://github.com/astrochart/CHART

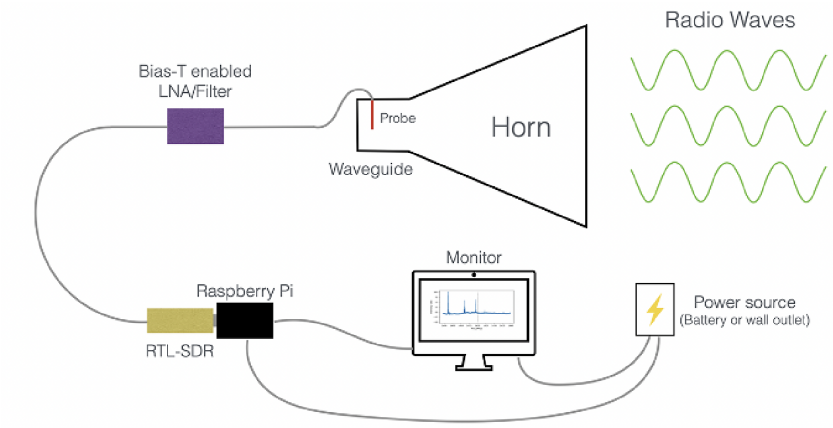

Figure 1: Experimental setup (from (Berkhout et al. 2023))

ranges and forcing the medians of the overlap regions to match, which removed small amplitude discontinuities between chunks.

Pointings. For each observing session, multiple trials were recorded for each unique sky direction. These pointings were logged using their celestial coordinates (sometimes approximately). For the Day 4 detections, the precise coordinate pairs used during the successful 21 cm observations are given in Table 1.

3. Observation Log

Day 1: Cardboard Horn on Sun and Galactic Plane Offset

The cardboard horn exhibited severe noise contamination. Pointings included the Sun and a location $\sim 30^\circ$ off the Galactic plane. The received spectrum showed no discernible HI peak and contained broad-band excess structure. Initial hypotheses included electronic noise coupling from the car, the monitor, and environmental RFI, which was hypothesized to be coming from a very large array of solar panels. This structure was right next to the set up, and was likely within the beam in several pointings.

No follow-up diagnostics were carried out on this day because it was the first interaction with the full setup.

Day 2: Metal Horn + FieldFox Diagnostics on ISTB4 Rooftop

Hypotheses from Day 1 were tested. Turning the monitor on/off showed no spectral change, rejecting that hypothesis. The metal horn replaced the cardboard horn, but despite improved SNR, no HI peak was visible at 1420 MHz. Multiple pointings directly through the Galactic plane yielded no detection. Environmental RFI at the rooftop may have contributed, but the root cause remained unclear.

Day 3: Raspberry Pi + Metal Horn (Still Untuned)

Experiments were repeated between ISTB4 and the parking garage. The switch to the Pi+SDR setup produced cleaner spectra with substantially improved SNR relative to Day 1. Two Galactic plane pointings were attempted. No peak was detected at 1420 MHz, but the baseline

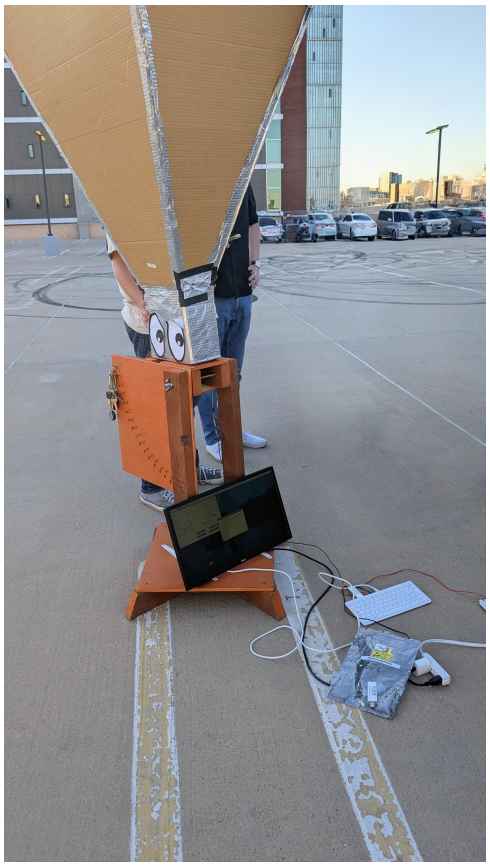

Figure 2: Day 1 setup with cardboard horn.

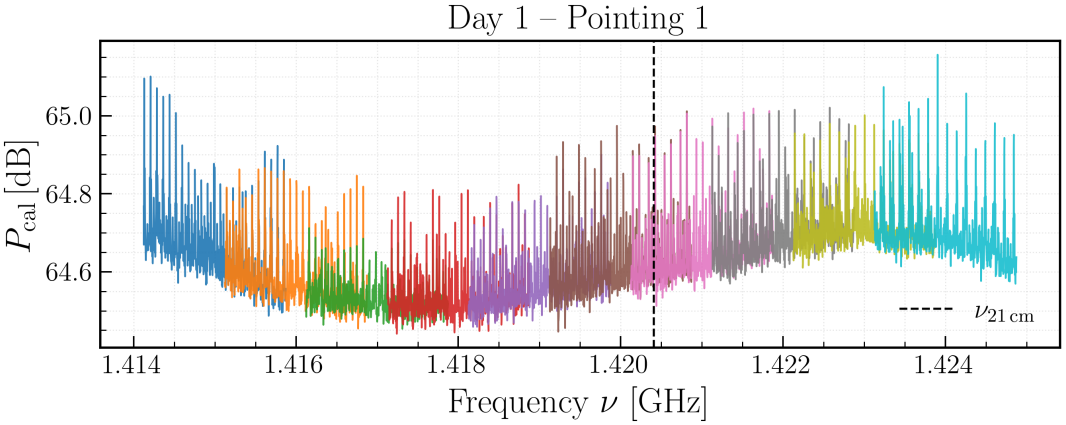

Figure 3: Day 1 spectra for pointing at 30 degree from galactic plane.

(a) Measured RFI spectrum inside the ISTB4 lab using the FieldFox analyzer, showing several narrowband interference peaks across the band.

(b) Example Day 2 rooftop observation toward the Galactic plane. Despite clear line-of-sight and improved setup, no 21 cm peak is visible in the extracted spectrum.

Figure 4: Day 2 diagnostics: comparison of the indoor RFI environment (left) with outdoor Galactic-plane observations from the ISTB4 rooftop (right).

stability was far superior, confirming that the cardboard horn was a major source of degradation.

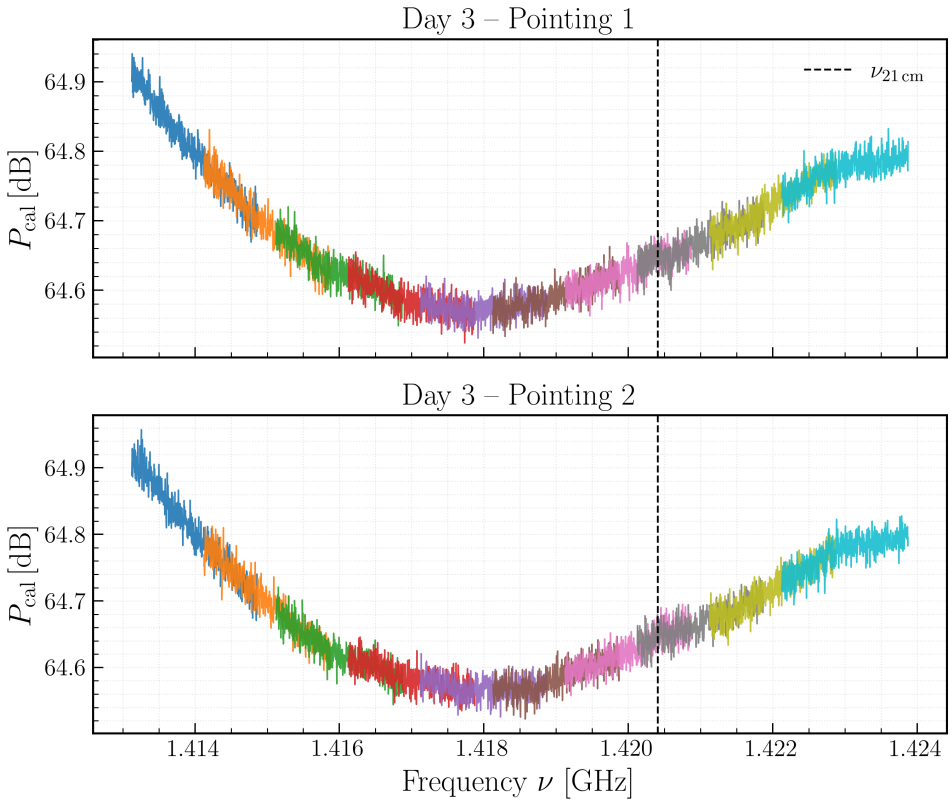

Figure 5: Day 3 stacked, calibrated spectra for all pointings (10 s integration, 5 iterations/bin).

Later inspection revealed the cause: the feed was resonant at ∼900 MHz, leading to heavy power reflection.

Day 4: Feed Retuned to 1420 MHz and Successful Detection

After cutting the probe wire to achieve resonance at 1420 MHz, return-loss measurements indicated $\sim 1\%$ reflection instead of $\sim 70\%$. Three pointings were performed.

Pointing 1. A faint peak near 1420 MHz appeared. The line was shallow, likely because the pointing was not accurately aligned with the Galactic plane. A strong, unexplained peak at ~ 1.415 GHz appeared. Hypothesis: RFI from a phone held within the beam. Retesting with all phones off eliminated the feature, confirming the possible RFI origin (although not with 100 percent certainity).

Pointing 2 (Corrected Pointing). Precise alignment produced a significant 21 cm detection at the correct rest frequency. The measured line width is approximately 15–20 $\mathrm{km\,s^{-1}}$, consistent with expected Galactic HI profiles combining thermal, turbulent, and rotation contributions.

Pointing 3 (Longer Integration). Doubling the number of iterations strengthened the detected line in dB. The continuum level also increased, consistent with longer averaging and slight frequency-dependent gain drift.

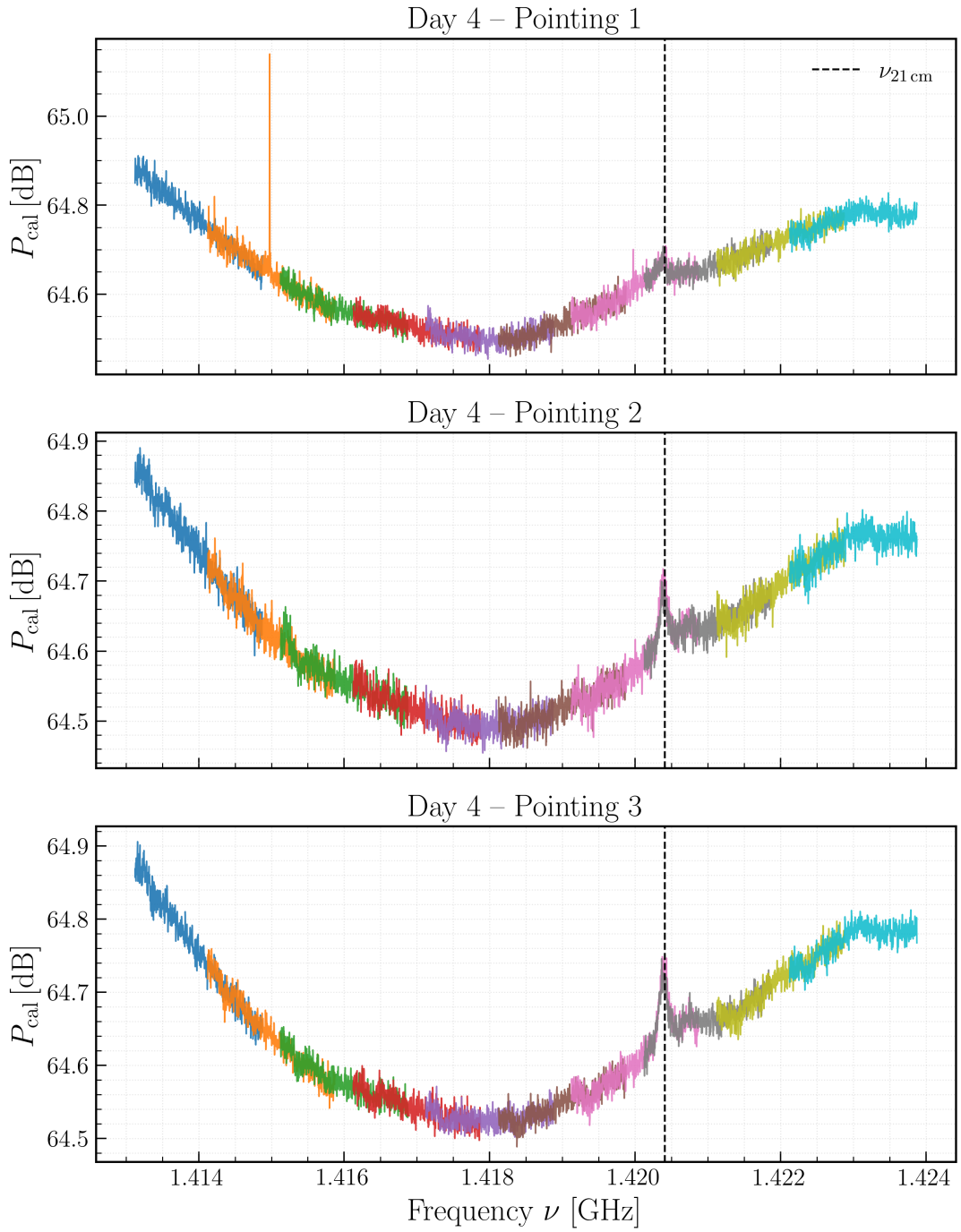

Figure 6: Day 4 calibrated spectra for all three pointings. The first pointing shows a faint 21 cm peak along with an RFI feature near 1.415 GHz, likely due to my phone inside the beam. After correcting the pointing, the second spectrum shows a Galactic 21 cm detection with a well-defined line shape. The third spectrum, obtained with doubled integration time, produces a stronger line amplitude but also an elevated continuum level.

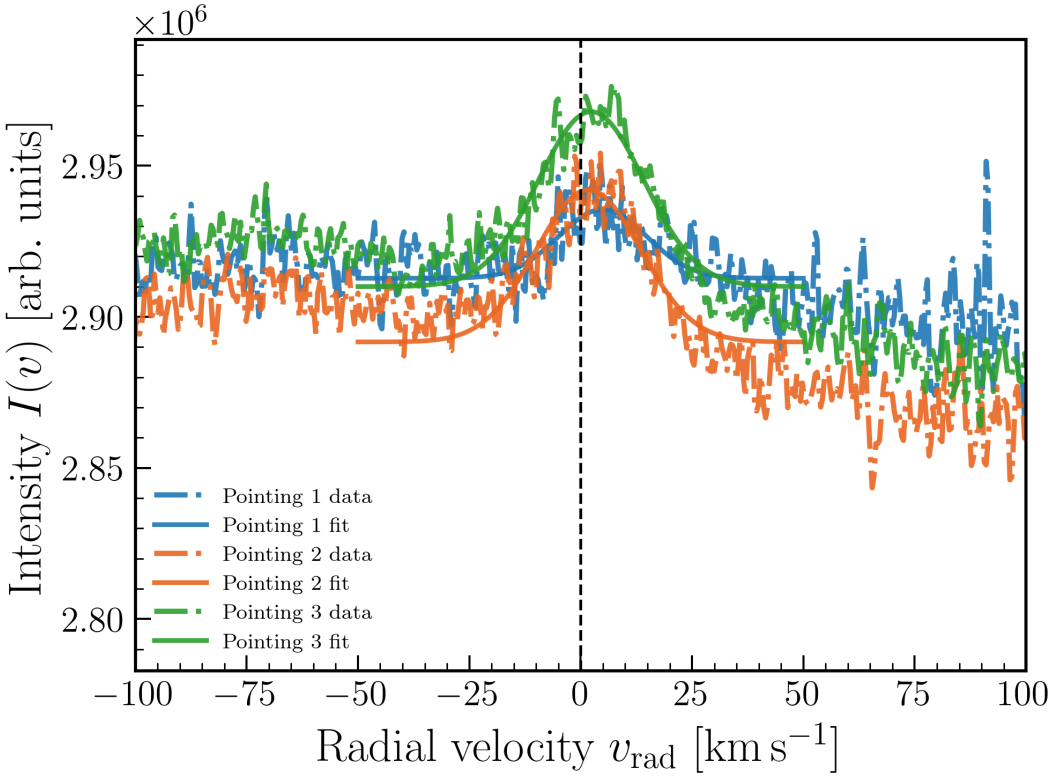

Figure 7: Day 4 corrected pointing: velocity-calibrated 21 cm profile showing a detection marked by a gaussian fit.

Pointing Coordinates and Fits (Day 4 only)

Table 1: Pointing coordinates for Day 4 detections (estimated from Stellarium; horn FOV ∼20°).

Pointing	RA (J2000)	Dec (J2000)	Notes
1	∼20h 20m (305°)	∼+48°	faint 21 cm peak + RFI at 1.415 GHz
2	∼19h 50m (297°)	∼+42°	corrected pointing; clear 21 cm detection
3	∼19h 10m (288°)	∼+30°	long integration; stronger line + raised continuum

Table 2: Gaussian line–fit parameters for the Day 4 21 cm detections. Fits were restricted to the velocity window $|v| \leq 50\ \mathrm{km\,s^{-1}}$. FWHM values correspond to the velocity dispersion along the line of sight.

Pointing	Line centre μ ($\mathrm{km\,s^{-1}}$)	FWHM ($\mathrm{km\,s^{-1}}$)	Peak amplitude A (arb. units)
1	4.94 ± 0.77	23.35 ± 2.13	$(2.28 \pm 0.16) \times 10^4$
2	1.77 ± 0.45	27.62 ± 1.31	$(5.04 \pm 0.18) \times 10^4$
3	2.36 ± 0.33	27.93 ± 0.96	$(5.79 \pm 0.15) \times 10^4$

Day 5: Observations

Continuing the way observations were done on day 4 we repeated the same experiment for a total of 4 different pointings on Day 5. We varied the number of iterations to average over,

the total integration time for each iteration and also the total bandwidth to be considered. Corresponding processed spectra are shown in Fig. 8 and the corresponding velocity space spectra with Gaussian fits in Fig. 9

Table 3: Same as Table 2 but for Day 5 pointings.

Pointing	Line centre μ ($\mathrm{km\,s^{-1}}$)	FWHM ($\mathrm{km\,s^{-1}}$)	Peak amplitude A (arb. units)
1	-2.138 ± 0.404	27.596 ± 1.184	$(3.537 \pm 0.115) \times 10^4$
2	-6.695 ± 0.742	56.609 ± 4.950	$(3.080 \pm 0.224) \times 10^4$
3	-0.494 ± 0.441	27.958 ± 1.300	$(3.302 \pm 0.116) \times 10^4$
4	-2.601 ± 0.548	32.063 ± 1.752	$(2.583 \pm 0.102) \times 10^4$

Table 4: Pointing coordinates for Day 5 detections (estimated from Stellarium).

Pointing	RA (J2000)	Dec (J2000)
1	$\sim$20h 22m (305°)	$\sim+40°$
2	$\sim$19h 30m (292°)	$\sim+25°$
3	$\sim$20h 45m (312°)	$\sim+33°$
4	$\sim$19h 50m (298°)	$\sim+35°$

5. Discussion

The progression across four days helped us isolate some limiting factors:

(a) Feed Mismatch - After day 3 of observations we had realized the feedline was mismatched with the intended tuned frequency of the HI line (1420 MHz), and instead optimized for 900 MHz. This caused significant loss ($\sim$70%) from the incident signal. The length of the probe coupled with the waveguide (the horn antenna) will set the antenna's impedance. In this case there was a mismatch between the antenna and the coaxial cable's characteristic impedance which caused significant reflections during the transmission of the signal. To fix this, the probe was trimmed to about half its original length, reducing the reflected signal to $\sim$1% at 1420 MHz.

(b) RFI Sources - Phones, vehicles, and uncontrolled campus electronics generate strong, narrowband peaks. The 1.415 GHz spike on Day 4 was traced directly to a phone inside the main lobe. The setup for Day 1 could have introduced multiple potential sources of unwanted RFI. One was the monitor that was placed nearby the horn. We tested the significance of the monitor's RFI inside the lab and found that moderate interference to the measured spectrum, but only when the monitor was placed inside the horn. Another potential source of RFI was due to nearby cars, specifically the one we were using for our power supply. Lastly, observations were obtained on the roof of the parking garage nearby ($\sim$80 feet) solar panels where the inverters or cabling could have produced significant RFI. To test this in the future we could to conduct the same experiment on the roof at different times of the day. Observations can be taken at night and day to see if the change in power output from the solar panels can

(c) Mechanical Pointing Accuracy - A horn with $\sim 20°$ FWHM beam requires careful alignment for maximum Galactic-plane brightness. Even small offsets degrade the signal when combined with gain and bandpass uncertainties.

(d) Integration Time Improves SNR- The 10 s $\times$ 5-bin Pi configuration and later doubled-integration tests demonstrate the classic $\sqrt{N}$ improvement in noise, though continuum offsets also increase.

(e) Final Detection Is Physically Consistent - The 20–30 $\mathrm{km\,s^{-1}}$ FWHM aligns with

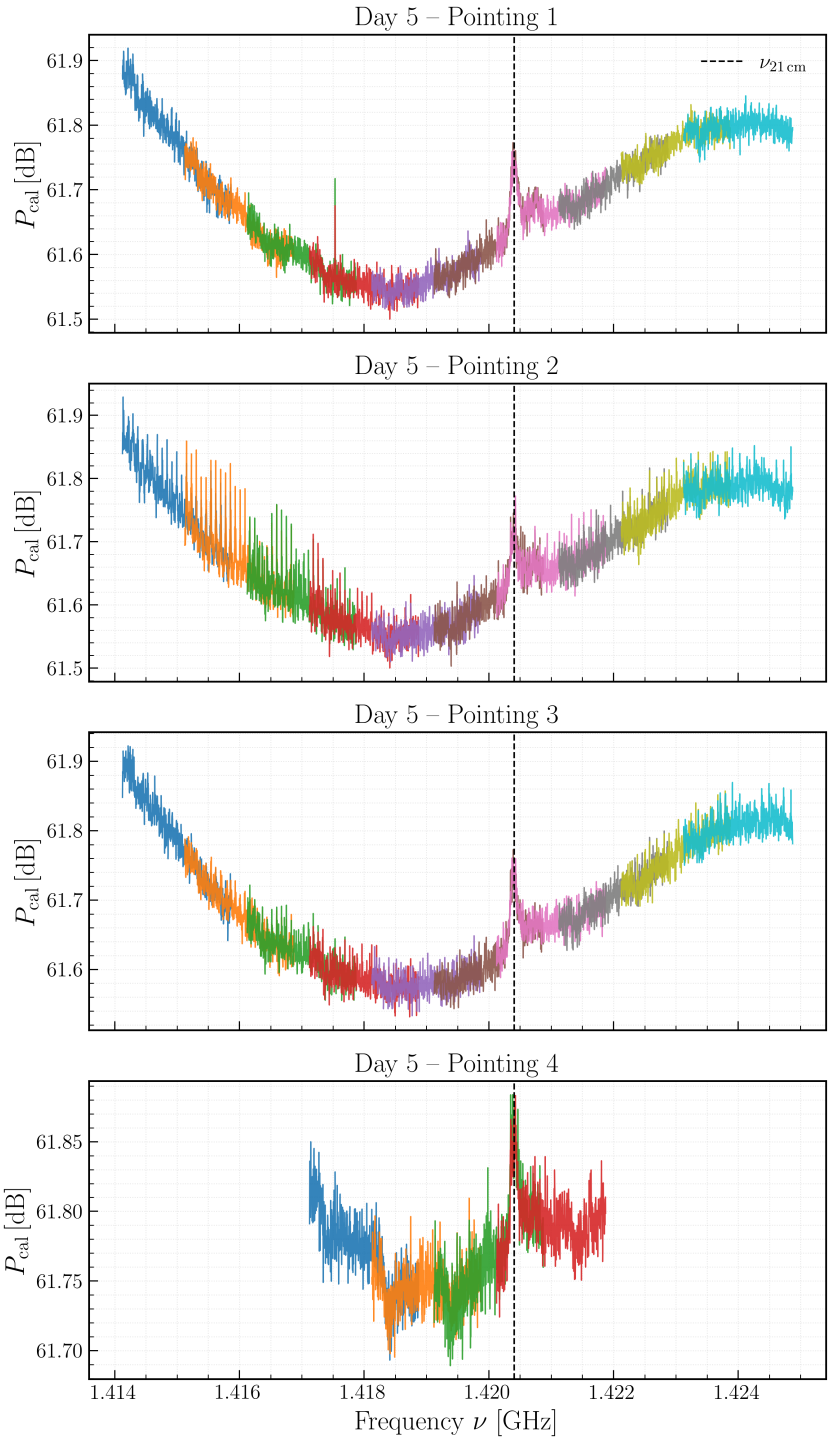

Figure 8: Day 5 calibrated spectra for all fourpointings.

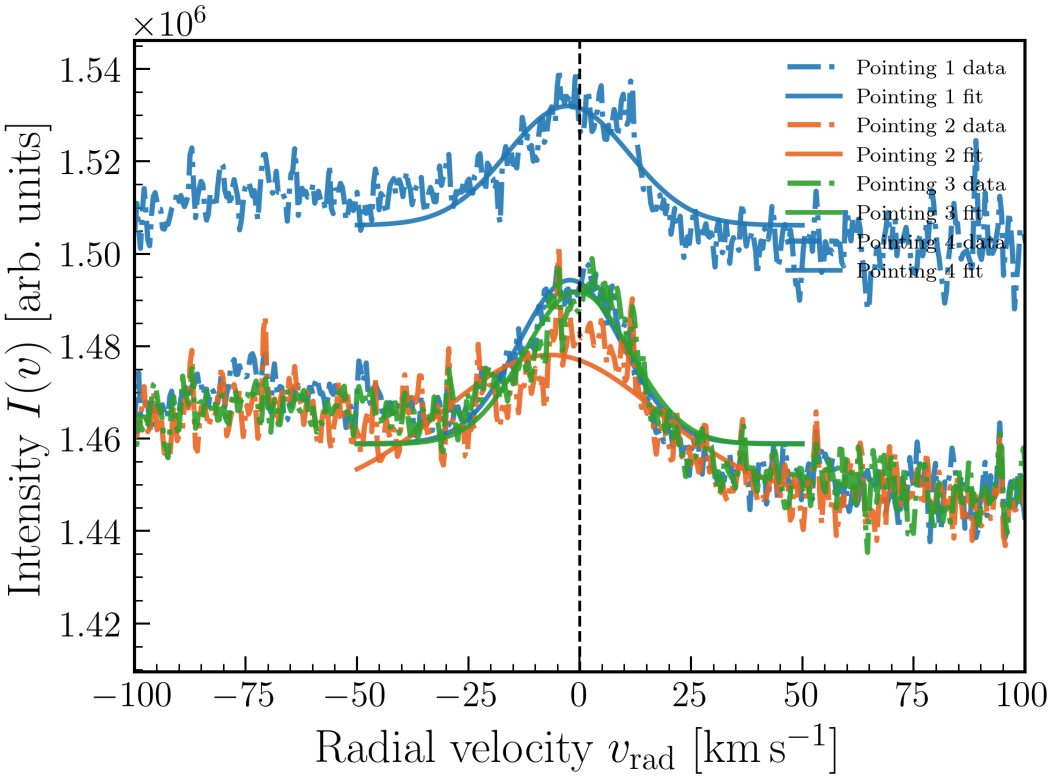

Figure 9: Day 5 corrected pointing: velocity-calibrated 21 cm profile showing a detection marked by a gaussian fit.

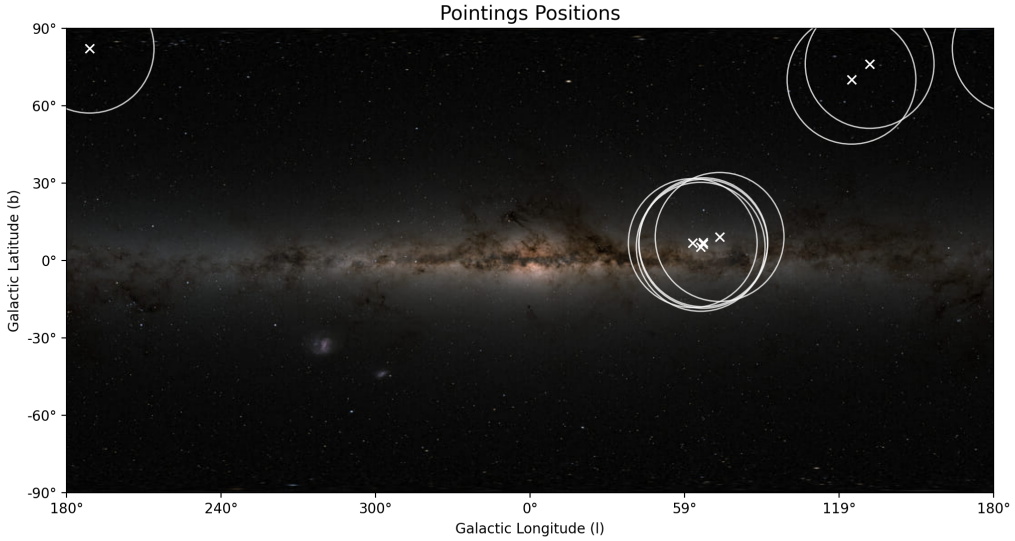

Figure 10: Map of positions for eight collected observations relative to the galactic plane, shown in the optical. We note the use of galactic coordinates in this figure. Image credit: NASA.

typical warm neutral medium conditions and bulk velocity dispersion along the Galactic plane.

Overall, we developed our understanding of the probe and how the noise temperature related to our system (e.g. LNA, coaxial extension cords, time/place of observations, external monitors). Producing higher fidelity data required a complete understanding of the actual signal, how we could mitigate RFI, signal degradation (i.e. removing combing effects in our data from a loud signal saturating the entire bandpass), digitized it, and synthesizing the output into detectable physics.

6. Mapmaking

We attempt to produce two galaxy maps using information derived from our CHART horn observations. We first map flux to measure intensity of HI emission, expecting the most prominent signal to be concentrated at the galactic plane (galactic latitude of 0). Later, we map rotational velocities relative to the CHART horn line-of-sight for each pointing. Although many more observations would be required to complete a comprehensive all-sky mapping project as shown in previous course lectures, we find our eight collected scans to be sufficient for making general conclusions regarding the galaxy's motion, based on known theory. For flux mapping, the general process we followed to convert CHART observations to maps are detailed as follows:

1. Convert the local horizon coordinates of a given observation to a common equatorial reference frame. This is so that pointings from a variety of locations, times, and days can be combined sensibly.
2. Append the flux values derived from the spectra to a healpix map as point sources.
3. Convolve the point source map with a gaussian beam with FWHM of 20 degrees, similar to the actual pointing accuracy of the real horn.
4. Print and show everything.

Shown below in Figures 9 and 10, we see good agreement between the spatial location of our flux peaks and the location of the actual Milky Way. This suggests that our pointings are accurate, and that we are recovering true flux from the Milky Way.

For rotational velocity mapping, we expand on the unabridged CHART tutorial, using preexisting code to estimate 21 cm bump Doppler shift offsets, then creating the map as follows:

1. Convert galactic coordinates output by tutorial, as well as beam radius (assumed 25 degrees), to radians.
2. Create a grid using the Mollweide projection.
3. Mark all grid pixels inside the beam radius centered at each pointing.
4. Average overlapping radial velocities for grid pixels contained within more than one pointing.
5. Plot the result, marking beam centers (Figure 11).

The benefits to mapping these characteristics are twofold. First, it allows for diagnostics of overall galactic motion, creating a straightforward summary figure for both relative motion and

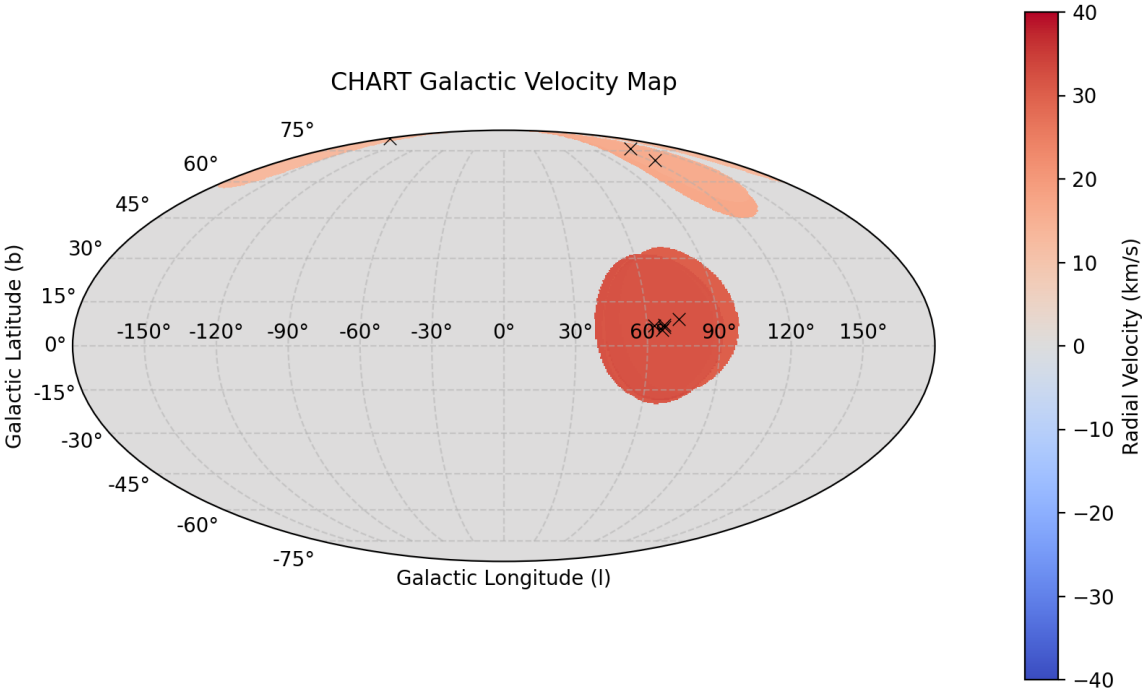

Figure 11: Map of line-of-sight velocities for eight collected observations at various points relative to the galactic plane. We note the use of galactic coordinates in this figure.

HI emission intensity. Second, it highlights possible sources of uncertainty in either experimental setup or data processing by highlighting observations that do not match theory.

To that extent, we utilize the Gaia mission line-of-sight velocities map (Figure 12) to evaluate the performance of our own, displaying the collective data of eight individual pointings in Figure 11. More observations at more varied galactic coordinates would be preferred, but were difficult to accomplish due to a combination of time and geographic constraints, as well as troubleshooting delays due to tuning.

We highlight the consistency between our measurements of radial velocity and similar areas in the Gaia map. We find velocities of approximately 30 km/s at the galactic plane, which is reasonable given both horn resolution and the Gaia measurements of approximately 20 - 30 km/s in the same area. Further, at higher latitudes we note lower velocities of approximately 5 - 10 km/s, consistent with Gaia observations which approach 0 km/s in the same areas (shown in green arching around the top of the map due to projection distortions). As a result, we reasonably conclude that our CHART measurements of radial velocity are meaningful and somewhat accurate to reality.

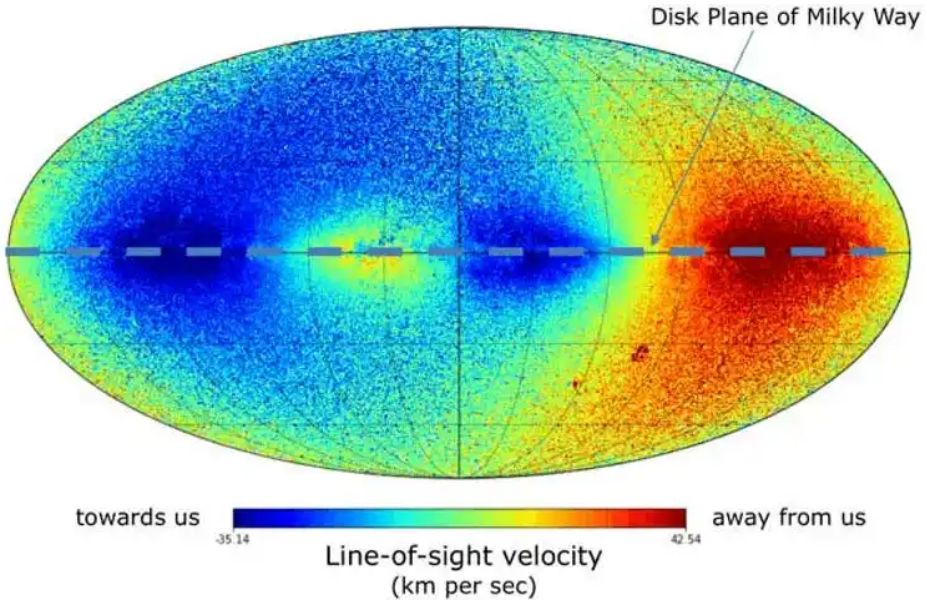

Figure 12: Map of line-of-sight velocities from the Gaia mission at superior resolution to our CHART horn. Credit: ESA.

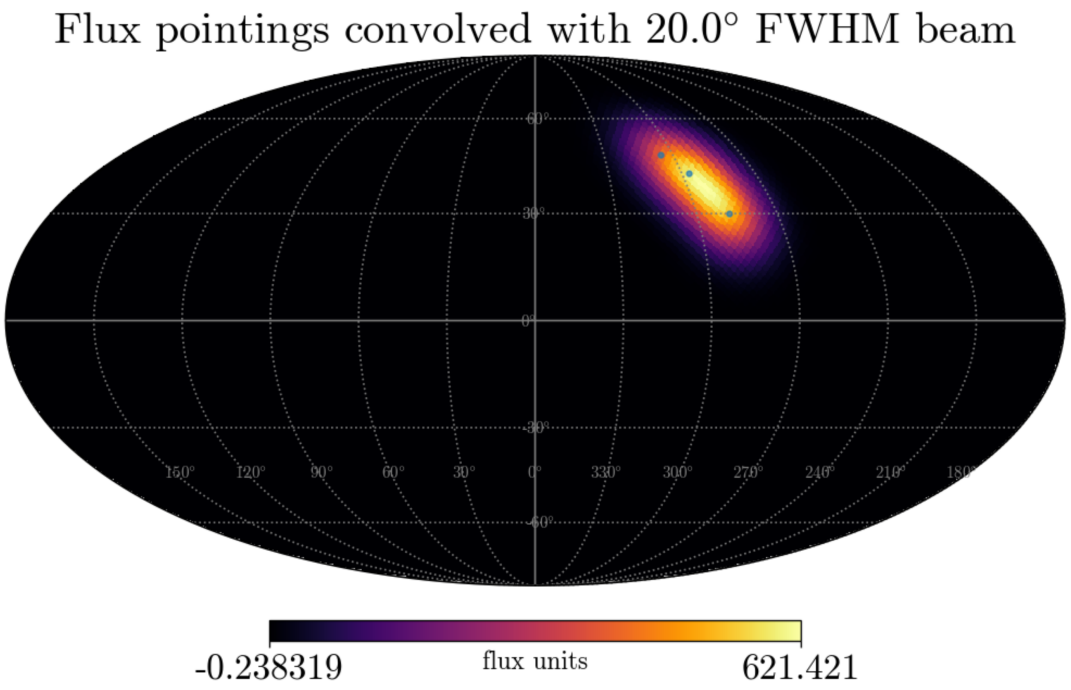

Figure 13: Example equatorial flux map generated with the three pointings detailed in Tables 1 and 2.

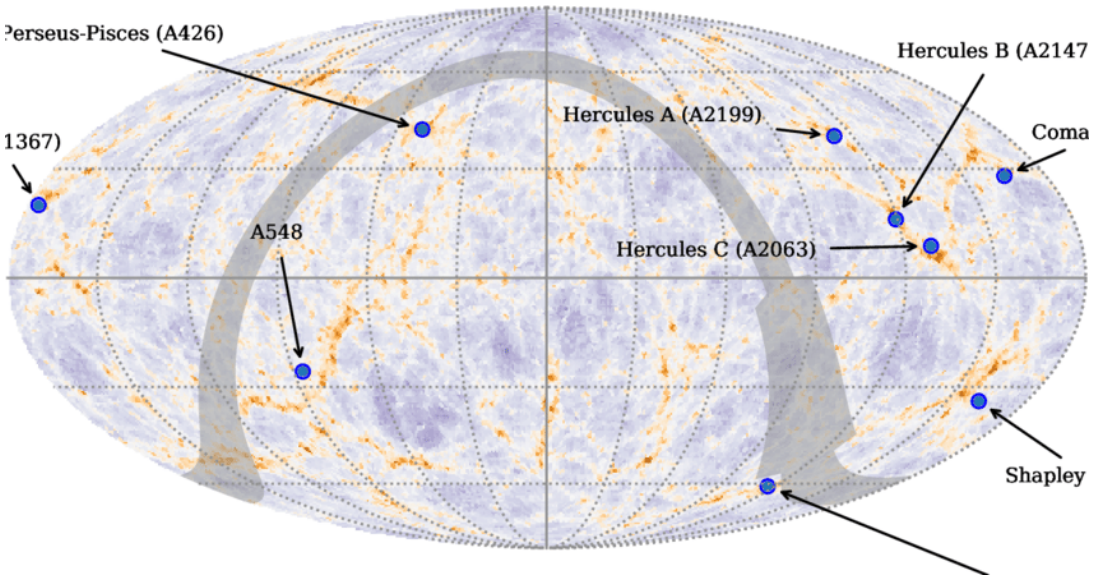

Figure 14: Equatorial Mollweide projection dark-matter map from Stopyra et al. 2019 with Milky Way zone-of-avoidance overshaded in gray. Close agreement with Figure 9 indicates we have genuine flux detected in the Milky Way.

7. Conclusion

Across four days of experimentation, we transitioned from complete non-detections to a clean recovery of the 21 cm Galactic HI line after identifying and correcting the dominant limitations: cardboard-horn inefficiency, feed-detuning, RFI contamination, and pointing uncertainty. The final tuned metal horn and Pi+SDR configuration successfully detected the line at the correct

frequency and with physically meaningful width.

Further, we demonstrate approximate consistency in radial velocity mapping with Gaia measurements, highlighting the physical significance of our observations and comparing the velocities of regions in the galactic plane and far from it. While more observations would improve confidence in these results, we find eight observations to be sufficient considering horn resolution and the repeatability of observations in similar regions (pointings in similar areas yielded similar radial velocities). Future work could explore running the experiment during the night

Credits

Tanmay Singh - Write up of Section 1, 2, 3, 4, 5. Taking observations on 5 different days for all the pointings as mentioned in Section 3. Figs. from 1 to 9. Table 1 to 4.

Sara Jones - Write up of Section 1, 2, 3, 4, 5. Taking observations on 5 different days for all the pointings as mentioned in Section 3. Figs. from 1 to 9. Table 1 to 4.

Tyler Karasinski - Write up of Section 6, 7, radial velocity mapping and associated figures, pointing positions map, CHART tutorial additions, and data processing using unabridged CHART tutorial.

Simon Mork - Section 6 write-up, equatorial flux map generation, and snippet for conversion between local azimuth coordinates to equatorial.

Ralph Ortiz - Helped take first two observations, reviewed codes written by Tyler and Simon, formatting of write up, contributions to Section 5, 6, and 7, attempted to create map of median absolute deviation of our measurements and noise for all pointings

Nick Foo - Contributions to Section 3, 5. Taking observations for 3 different days.

Devyn Podrybau- Contributions to Section 1 and references, helped take observations second day, final draft formatting

References

Basu, A., Roy, N., Beuther, H., et al. 2022, Monthly Notices of the Royal Astronomical Society, 517, 5063, doi: 10.1093/mnras/stac3043

Berkhout, L. M., Beardsley, A. P., Jacobs, D. C., et al. 2023, Physics Education, 59, 015020, doi: 10.1088/1361-6552/ad0542